σ-antibonding orbitals (a_{1g} and b_{1g}) and less vibronic coupling, resulting in more Laporte forbiddenness overall and relatively low molar absorptivities.

An $AuCl_2$ or $AlCl_2$ unit attached to an edge of an $AuCl_4$ unit would be expected to cause changes in the spectral region involving ligand-metal charge transfer compared to that for the $[AuCl_4]^-$ ion. However, $Au_2Cl_6(s)$ has energies very similar to those for the $^1A_{2u}, ^1E_u(1) \leftarrow {}^1A_{2g}$ and $^1E_u(2) \leftarrow {}^1A_{1g}$ transitions for $[AuCl_4]^-$, and $AlAuCl_6(g)$ has a similar transition to that of $^1E_u(2) \leftarrow {}^1A_g$. The apparent absence of a transition for both $Au_2Cl_6(g)$ and $AlAuCl_6(g)$ similar to $^1A_{2u}, ^1E_u(1) \leftarrow {}^1A_{1g}$ for $[AuCl_4]^-$ may be due to temperature effects on molar absorptivities. The charge-transfer molar absorptivities at the λ_{max}'s decrease and the bands broaden with increase in temperature, and this transition could be simply under the intense peak. Also, experimentally, this is the region where the chlorine absorbance is large and, thus, the largest subtraction uncertainties occur.

The $AlAuCl_6(g)$ spectrum shows only one absorption maximum for the most intense peak whereas $Au_2Cl_6(g)$ has two maxima. The λ_{max} for $AlAuCl_6(g)$ appears to be an average of those for $Au_2Cl_6(g)$. The areas, per gold atom, under the peaks are roughly the same. It appears that the 244-nm peak shifts to shorter wavelengths while the 222-nm peak shifts to longer wavelengths when one of the gold atoms in $Au_2Cl_6(g)$ is replaced by an aluminum atom. One explanation for this effect is to assume that one of the transitions for $Au_2Cl_6(g)$ involves the bridging chlorine atoms (244 nm) and the other involves the terminal chlorine atoms (222 nm).[17] Replacement of one of the Au(III) atoms with the stronger polarizing Al(III) atom (based on charge density)[18] causes the 244-nm transition to shift to shorter wavelengths. The resulting decrease in electron density on the remaining Au(III) atom causes the other transition to occur at longer wavelengths. The above assignment could be reversed and Al(III) could be less polarizing (based on Au(III) being a transition metal ion)[18] resulting in the same overall effect. However, replacing an electron on the $[AuCl_4]^-$ ion with an $AlCl_2$ or $AuCl_2$ unit should cause a significant shift to shorter wavelengths, just the opposite of that observed. Another explanation involves the bending of the bridge. Theoretical calculations[19] indicate that the two sets of d-orbitals in dimeric, square-planar complexes split depending on the "hinge" angle, and thus, two different transitions are possible. In the solid phase, Au_2Cl_6 molecular units are planar, but in the gas phase, the molecules are free to bend. With $AlAuCl_6(g)$, the tetrahedrally distributed chlorine atoms attached to the aluminum atom may stereochemically decrease the amount of bending.

The $AlAuCl_5(g)$ molecule supposedly has quite a different structure than those above. However, surprisingly, the derived spectrum correlates best with that of the $[AuCl_4]^-$ ion, except for the enhancement of the molar absorptivities of the d-d transitions. Also, λ_{max} for the intense charge-transfer band has shifted to a shorter wavelength, compared to $AlAuCl_6(g)$, as expected from the lower oxidation number on the gold atom.

Thermodynamic Constants. Equilibrium constants for reactions 1, 3, and 5 were calculated from the derived concentrations (Table S1, supplementary material). Least-squares treatments of ln K vs $1/T$ gave the constants listed in Table IV along with the corresponding thermodynamic constants. The $\Delta H°$ and $\Delta S°$ values for reactions 1 and 3, from I and II, agree within the experimental uncertainty. Enthalpy of formation and standard entropy values for $AlAuCl_6(g)$ and $AlAuCl_5(g)$ were calculated using reference data from the sources cited in the table. The entropy projected for $AlAuCl_6(g)$ when II is used is 8 J K^{-1} mol^{-1} less than when I is used. The difference, $S°(AlAuCl_6(g)) - S°(AlAuCl_5(g))$, 87 J mol^{-1} K^{-1}, is somewhat larger than found for simpler pairs of molecules which differ by one chlorine atom, e.g. $S°(FeCl_3(g)) - S°(FeCl_2(g))$ = 60 J mol^{-1} 1 K^{-1}.[9]

The results derived for reaction 1 are compatible with those expected on statistical grounds. The enthalpy change is small, and the equilibrium constant is of the order of unity; e.g. at 600 K, K_1(I) is 2.4 and K_1(II) is 1.1.

Supplementary Material Available: Table S1, a detailed listing of temperatures, observed absorbances, and derived concentrations for the various samples (3 pages). Ordering information is given on any current masthead page.

(17) Mason, W. R.; Gray, H. B. *J. Am. Chem. Soc.* **1968**, *90*, 5721.
(18) Huheey, J. E. *Inorganic Chemistry, Principles of Structure and Reactivity*, 2nd ed.; Harper and Row: New York, 1978; pp 91-92.
(19) Summerville, R. H.; Hoffmann, R. *J. Am. Chem. Soc.* **1976**, *98*, 7240.
(20) Barin, I. *Thermochemical Data of Pure substances*; VCH Publishers: New York, 1989.

Contribution from the Instituto de Química-UNESP, Caixa Postal 355, 14800 Araraquara, SP-Brazil, Instituto de Física e Química-USP, Caixa Postal 369, 13560 São Carlos, SP-Brazil, and Department of Chemistry, Washington State University, Pullman, Washington 99164-4630

Synthesis, Structure, and Electronic and EPR Spectra of Copper(II) Complexes Containing the $[CuBr_4]^{2-}$ Anion and Triphenylarsine Oxide

Antonio Carlos Massabni,† Otaciro Rangel Nascimento,‡ Kristopher Halvorson,§ and Roger D. Willett*,§

Received June 11, 1991

The preparation and characterization of $(Ph_3AsOH)_2[CuBr_4]$ and $[Cu(Ph_3AsO)_4][CuBr_4]$ are reported (Ph_3AsO = triphenylarsine oxide). Crystallographic analysis of the monoclinic crystals of $(Ph_3AsOH)_2[CuBr_4]$ (space group $C2/c$, a = 17.569 (3) Å, b = 13.090 (2) Å, c = 16.933 (2) Å, and β = 105.64 (2)°, R = 0.055 and R_w = 0.057) revealed the presence of compressed $[CuBr_4]^{2-}$ tetrahedra of C_2 symmetry with Cu-Br distances of 2.340 (1) and 2.437 (1) Å and *trans*-Br-Cu-Br angles of 139.2 (1) and 122.4 (1)°. The oxonium cations hydrogen bond to the bromine atoms involved in the longer Cu-Br bonds and the smaller *trans*-Br-Cu-Br angle. Single-crystal electronic and EPR spectra are interpreted in terms of the observed $[CuBr_4]^{2-}$ geometry. Analysis of the electronic and EPR spectra of $[Cu(Ph_3AsO)_4][CuBr_4]$ led to the postulation of the presence of planar $[Cu(Ph_3AsO)_4]^{2+}$ cations and distorted tetrahedral $[CuBr_4]^{2-}$ anions.

Introduction

Copper(II) complexes with phosphine and arsine oxides, mainly Ph_3AsO, have been obtained and studied in one of our laboratories. Square-planar complexes containing the cation $[Cu(Ph_3AsO)_4]^{2+}$ and the anions ClO_4^-, NO_3^-, and $[Cu^ICl_2]^-$ were previously described.[1] Compounds with the anion $[CuX_4]^{2-}$ (X = Cl^-, Br^-) were also studied.[2] In the presence of strong acid, protonation

† Instituto de Química-UNESP.
‡ Instituto de Física e Química-USP.
§ Washington State University.

(1) Nascimento, O. R.; Massabni, A. C. *Polyhedron* **1985**, *4*, 707.
(2) (a) Massabni, A. C.; Nascimento, O. R.; Almeida Santos, R. H.; Francisco, R. H. P.; Lechat, J. R. *Inorg. Chim. Acta* **1983**, *72*, 127. (b) Halvorson, K. E.; Willett, R. D.; Massabni, A. C. *J. Chem. Soc., Chem. Commun.* **1990**, 346.

0020-1669/92/1331-1779$03.00/0

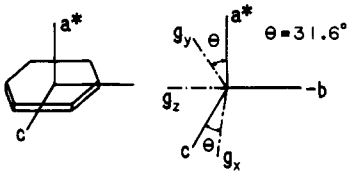

Figure 1. Schematic drawing showing the habit of the crystal utilized to measure EPR and polarized electronic spectra.

of the oxide occurs with the formation of Ph_3ZOH^+ or $(Ph_3ZO)_2H^+$ species (Z = P, As).[2]

In the present paper we wish to describe synthesis, crystal structure, and spectroscopic properties of the two complexes $CuBr_2 \cdot 2HBr \cdot 2Ph_3AsO$ (purple) and $[Cu(Ph_3AsO)_4][CuBr_4]$ (olive green). The first complex is better formulated as $(Ph_3AsOH)_2[CuBr_4]$.

Preliminary observations about the properties of these two complexes were reported by Goodgame and Cotton a number of years ago.[3] They described the preparation of a complex formulated as $CuBr_2 \cdot 2Ph_3AsO$ which was purple when freshly prepared, but the color changed to olive green when dried.

Experimental Section

Preparation of the Complexes. $(Ph_3AsOH)_2[CuBr_4]$. A suspension of $CuCO_3 \cdot Cu(OH)_2 \cdot nH_2O$ in ethanol was treated with 48% HBr until total dissolution of the solid occurred. The resulting solution was warmed on a hot plate and mixed with a hot ethanolic solution of Ph_3AsO. A molar proportion of 1 Cu to 2 Ph_3AsO was used. The mixture was boiled for a few minutes and cooled at room temperature. Well-developed purple crystals were precipitated after addition of some drops of 48% HBr into the solution. The crystals were filtered off and washed with ether. They are stable when kept at 110 °C and when left in a desiccator over P_4O_{10} or $CaCl_2$. The crystals melted at 153–155 °C. Anal. Calcd: Cu, 6.17; C, 41.98; H, 3.11; Br, 31.06. Found: Cu, 6.40; C, 42.6; H, 3.21; Br, 31.05. Cu^{2+} was determined with 0.010 M EDTA and Br by gravimetric analysis with $AgNO_3$. The complex was previously dissolved in hot ethanol, and boiling water was added to the ethanolic solution for decomposition.

$[Cu(Ph_3AsO)_4][CuBr_4]$. This complex was prepared by following the same procedure as above but without addition of 48% HBr. The olive green solid precipitated immediately (mp 240–241 °C). Anal. Calcd: C, 49.8; H, 3.46. Found: C, 47.9; H, 3.51.

Electronic Spectra. The electronic spectra of the powder compounds were recorded on a Cary 17 spectrophotometer as mulls with fluorolube oil for the wavelength ranges 300–800 and 750–2000 nm for the olive green complex and 300–700 nm for the purple complex. A single crystal of the purple complex was mounted in a Beckman DK2 spectrophotometer, and polarized spectra were recorded in the range 800–1600 nm.

EPR Spectra. The EPR spectra were obtained using a Varian E-109 X-band spectrometer for both powder and single-crystal samples. A cylindrical cavity was used in the measurement of angular variation of the single-crystal spectra. The crystal habit, illustrated in Figure 1, exhibits the well-developed (100) faces. The spectra were recorded at room temperature in three mutually perpendicular planes with one plane normal to the b axis and a second normal to the a^* axis.

X-ray Data. A thin opaque crystal of the triphenylarsine oxonium salt with the (100) faces well developed and a maximum dimension of 0.3 mm was mounted on a glass fiber for data collection. Data were collected on a Syntex $P2_1$ diffractometer system upgraded to Nicolet P3F specifications, with Mo Kα radiation (λ = 0.71069 Å) and a graphite monochromator.[4] All crystallographic calculations were carried out with the SHELXTL package[5] on a Data General Eclipse computer. Empirical absorption corrections were made by assuming a laminar-shaped crystal, utilizing the routine XEMP. Intensity statistics suggest that the space group is the centrosymmetric group $C2/c$. Direct methods, utilizing the routine SOLV, yielded the positions of the Cu, Br, and As atoms. Subsequent difference maps, starting with these positions, yielded all other atom positions. Refinement on F via a cascading block-diagonal least-squares algorithm with anisotropic thermal parameters for the non-carbon and non-hydrogen atoms and isotropic thermal parameters for carbon and hydrogen atoms (fixed values approximately 20% larger than the corresponding heavy atoms) gave a final value of $R = 0.0553$ and $R_w = 0.0568$ for all observed reflections with $|F_o|$ greater than $3\sigma(F_o)$, where $R = \sum||F_o| - |F_c||/\sum|F_o|$ and $R_w = \sum w(|F_o| - |F_c|)^2/\sum w|F_o|^2$ with $w = \sigma^2(F_o) + g|F_o|^2$. The phenyl rings were refined as rigid bodies, and attached hydrogens were placed at calculated distances. The positional parameters for the cationic proton were varied. Scattering factors were supplied by XHELXTL. Crystal parameters are summarized in Table I. Final positional parameters are given in Table II with selected bond distances and angles reported in Table III.

(3) Goodgame, D. M. L.; Cotton, F. A. *J. Chem. Soc.* **1961**, 2298.
(4) Campana, C. F.; Shepard, D. F.; Litchman, W. N. *Inorg. Chem.* **1981**, *20*, 4039.
(5) Sheldrick, G. SHELXTL Version 5.1. Nicolet Instrument Corp., 1986.

Table I. Crystallographic Data for $(Ph_3AsOH)_2[CuBr_4]$

$C_{36}H_{32}As_2Br_4CuO_2$	fw 1029.7
a = 17.569 (3) Å	space group $C2/c$ (No. 15)
b = 13.090 (2) Å	λ = 0.71069 Å
c = 16.933 (2) Å	ρ_{calcd} = 1.82 g cm^{-3}
β = 105.64 (2)°	μ = 65.8 cm^{-1}
V = 3750 (1) Å^3	transm coeff = 0.055–0.872
Z = 4	$R(F_o)$ = 0.055 (0.083, all data)[a]
T = 22 °C	$R_w(F_o)$ = 0.057 (0.064, all data)[b]

[a] $R = \sum||F_o| - |F_c||/\sum|F_o|$. [b] $R_w = \sum w(|F_o| - |F_c|)^2/\sum w|F_o|^2$.

Table II. Atomic Coordinates (×10^4) and Isotropic Thermal Parameters[a] (×10^3) for $(Ph_3AsOH)_2[CuBr_4]$

atom	x	y	z	U, Å^2
Cu	0	2745 (1)	2500	44 (1)
Br(1)	813 (1)	1849 (1)	1763 (1)	55 (1)
Br(2)	991 (1)	3368 (1)	3612 (1)	67 (1)
As	1616 (1)	−685 (1)	2860 (1)	39 (1)
O	894 (4)	63 (6)	3065 (5)	54 (3)
H(01)	763 (6)	588 (8)	2716 (7)	64
C(11)	2632 (4)	909 (5)	3674 (5)	46 (5)
C(12)	3359 (4)	1343 (5)	4071 (5)	64 (6)
C(13)	4055 (4)	794 (5)	4144 (5)	77 (7)
C(14)	4023 (4)	−190 (5)	3820 (5)	78 (7)
C(15)	3296 (4)	−624 (5)	3423 (5)	48 (5)
C(16)	2600 (4)	−75 (5)	3350 (5)	41 (4)
C(21)	650 (3)	−1079 (6)	1256 (5)	57 (5)
C(22)	486 (3)	−1170 (6)	406 (5)	63 (6)
C(23)	1086 (3)	−1033 (6)	20 (5)	63 (6)
C(24)	1852 (3)	−806 (6)	484 (5)	69 (6)
C(25)	2017 (3)	−714 (6)	1334 (5)	56 (5)
C(26)	1416 (3)	−851 (6)	1720 (5)	38 (4)
C(31)	1516 (5)	−1889 (5)	4224 (4)	56 (5)
C(32)	1401 (5)	−2788 (5)	4619 (4)	72 (6)
C(33)	1260 (5)	−3704 (5)	4184 (4)	68 (6)
C(34)	1233 (5)	−3722 (5)	3353 (4)	93 (8)
C(35)	1348 (5)	−2823 (5)	2957 (4)	70 (6)
C(36)	1489 (5)	−1907 (5)	3393 (4)	43 (5)

[a] Equivalent isotropic U values defined as one-third of the trace of the orthogonalized U_{ij} tensor.

Table III. Bond Distances (Å) and Angles (deg) for $(Ph_3AsOH)_2[CuBr_4]$

Distances			
Cu–Br(1)	2.437 (1)	As–C(26)	1.880 (1)
Cu–Br(2)	2.340 (1)	As–C(36)	1.879 (1)
As–O	1.711 (1)	O–H(01)	0.896 (1)
As–C(16)	1.881 (1)		

Angles			
Br(1)–Cu–Br(2)	99.7 (1)	C(16)–As–C(36)	111.3 (1)
Br(1)–Cu–Br(1a)	122.4 (1)	C(26)–As–C(36)	112.4 (1)
Br(1)–Cu–Br(2a)	99.6 (1)	As–C(16)–C(11)	120.0 (1)
Br(2)–Cu–Br(2a)	139.2 (1)	As–C(16)–C(15)	119.9 (1)
O–As–C(16)	108.1 (1)	As–C(26)–C(21)	119.3 (1)
O–As–C(26)	109.3 (1)	As–C(26)–C(25)	120.7 (1)
C(16)–As–C(26)	113.4 (1)	As–C(36)–C(31)	119.6 (1)
O–As–C(36)	101.5 (1)	As–C(36)–C(35)	120.4 (1)

Results and Discussion

Structure Description. The structure of the purple compound, $(Ph_3AsOH)_2[CuBr_4]$, consists of discrete $[CuBr_4]^{2-}$ anions and Ph_3AsOH^+ cations (Figure 2a). The copper ion, which sits on a site of C_2 symmetry, has a compressed tetrahedral geometry. The Cu–Br(1) and Cu–Br(2) bond lengths are 2.437 (2) and 2.340

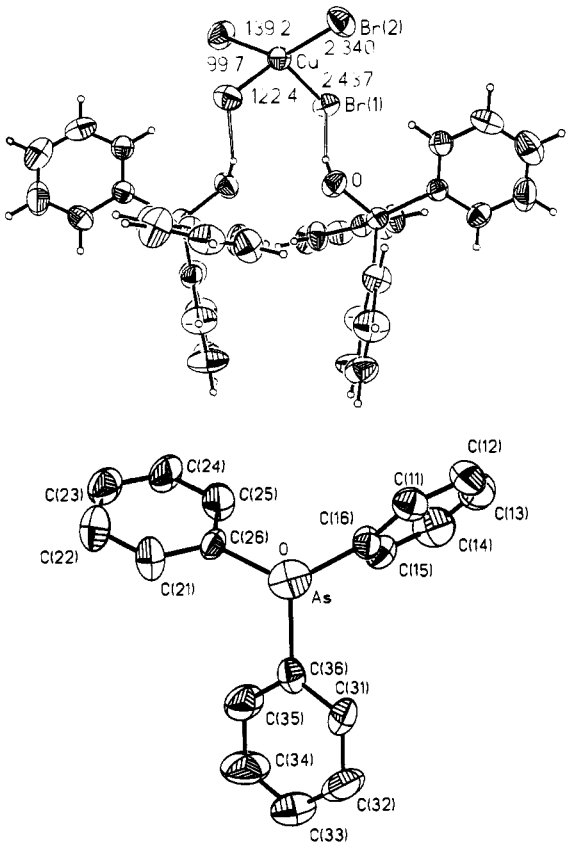

Figure 2. (a) Top: Illustration of the $(Ph_3AsOH)_2[CuBr_4]$ species. The *b* axis is vertical. (b) Bottom: Illustration of the (Ph_3AsO) fragment as view down the As–O bond.

(1) Å, respectively. The bond angles are 99.7 (1)° for Br(1)–Cu–Br(2), 122.4 (1)° for Br(1)–Cu–Br(1), 99.6 (1)° for Br(1)–Cu–Br(2), and 139.2 (1)° for Br(2)–Cu–Br(2). The cation hydrogen bonds to the anion through O–H···Br(1) interactions (Figure 2a). The effect of hydrogen bonding upon the $[CuBr_4]^{2-}$ geometry is clearly seen. This oxonium hydrogen bond to Br(1) causes the Cu–Br bond to be nearly 0.1 Å longer than the corresponding bond to Br(2). Also, the packing of the oxonium ions (Figure 2a) causes the *trans*-Br(1)–Cu–Br(1) angle to reduce to the 122.4° value, 16.8° smaller than the *trans*-Br(2)–Cu–Br(2) angle. The $[CuBr_4]^{2-}$ ion, with site symmetry C_2, has nearly a C_{2v} geometry, since the dihedral angle between the $CuBr_2$ planes containing the trans angles is 90.5°. The C_2 axis lies parallel to the crystallographic *b* axis, while the normals to the Br(1)–Cu–Br(1a) and Br(2)–Cu–Br(2a) planes make angles of 47.1 and 137.6° with the *c* axis. Thus, the $[CuBr_4]^{2-}$ anion lies athwart the *bc* plane. Local *x* and *z* axes are thus defined so as to lie parallel to the normal Br(1)–Cu–Br(1a) plane and the crystallographic *b* axis, respectively, with the *y* axis normal to these two directions. The closest interionic Br···Br contact is 6.48 Å, thus ensuring that neighboring monomers are well isolated from each other.

It is well established that $[CuCl_4]^{2-}$ anions show a more or less continuous range of geometries in which the *trans*-Cl–Cu–Cl angles range from about 125 to 180°.[6] The latter corresponds to a square-planar coordination geometry. This variability in trans angle is rationalized in terms of the balance between crystal field stabilization (favoring the square-planar limit) and ligand–ligand repulsions (favoring the tetrahedral limit). Factors which remove charge from the ligands, such as hydrogen bonding, will normally lead to preferential formation of species near the square-planar limit. A similar trend may be expected for the $[CuBr_4]^{2-}$ anions. A search of the literature,[7] as well as data from unpublished

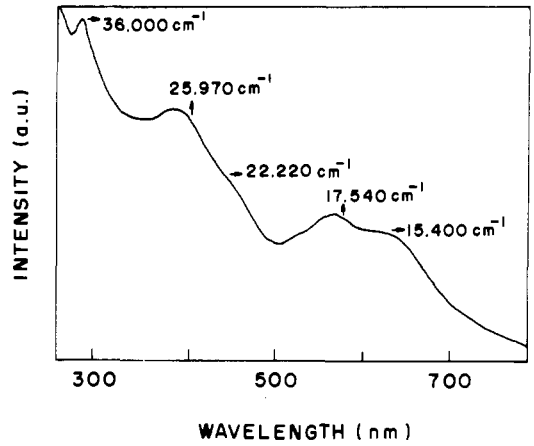

Figure 3. Electronic spectra of the $(Ph_3AsOH)_2[CuBr_4]$ complex in the region 300–800 nm (Fluorolube mull).

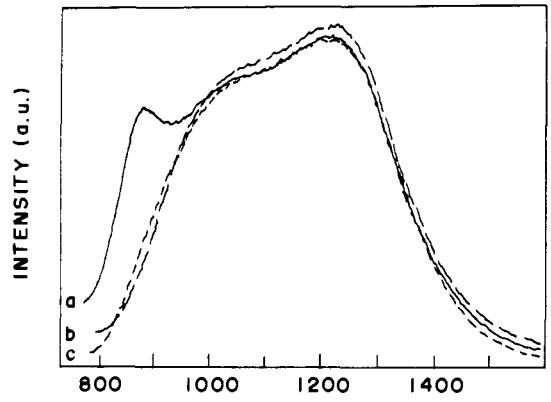

Figure 4. Electronic spectra of the $(Ph_3AsOH)_2[CuBr_4]$ crystal with polarized light in the near-infrared region: (a) $\vec{E}$ parallel to $\vec{b}$; (b) $\vec{E}$ perpendicular to $\vec{b}$; (c) unpolarized spectrum.

structures in one of our laboratories,[8] reveals trans angles ranging from 128.5 (the Me_4en^{2+} salt[8a]) to 142.1° (the *N*-methylphenethylammonium salt[7a]). The Ph_3AsOH^+ salt reported here falls in the lower end of the observed range. The lack of examples of isolated $[CuBr_4]^{2-}$ anions with geometries near the square-planar limit is probably due to the larger size of Br^- relative to Cl^-.

The cation, Ph_3AsOH^+, contains an arsenic atom with a geometry that is slightly distorted from tetrahedral (see Table III). The planes of the phenyl rings are twisted from the O–P–C plane by 11.9° for ring 1, by 46.3° for ring 2, and by 56.0° for ring 3, as seen in Figure 2b. The O–H distance was found to be 0.90 (11) Å, with an As–O–H bond angle of 113 (8)° and an O–H···Br angle of 162.2°. The hydrogen bonded O···Br distance is 3.191 Å, and the As–O···Br angle is 100.1°. The close O···O contact of 3.207 Å between neighboring Ph_3AsOH cations related by a 2-fold symmetry element is probably forced by the hydrogen bonding to the $[CuBr_4]^{2-}$ anion and not due to undetected O–H–O hydrogen bonding. For example, the Ph_3AsO–H–Ph_3AsO cation in $[(Ph_3AsO)_2H]_2Hg_2Br_6$ has an O···O distance of 2.40 Å.[9]

Electronic Spectra. The visible–UV spectrum of the $(Ph_3AsOH)_2[CuBr_4]$ complex (Figure 3) shows four bands in the

(6) Halvorson, K.; Patterson, C.; Willett, R. D. *Acta Crystallogr.* **1990**, *B46*, 508.

(7) (a) Place, H.; Willett, R. D. *Acta Crystallogr.* **1988**, *C44*, *34* and references therein. (b) Madariaga, G.; Alberdi, M. M.; Zuniga, F. J. *Acta Crystallogr.* **1990**, *C46*, 2363. (c) Boeyens, J. C. A.; Dobson, S. M.; Oosthuizen, E. L. *J. Cryst. Spectrosc. Res.* **1990**, *20*, 407. (d) Tosik, A.; Bukowska-Strzyzewska, M. *J. Cryst. Spectrosc. Res.* **1989**, *19*, 707. (e) Patyal, B. R.; Scott, B. L.; Willett, R. D. *Phys. Rev.* **1990**, *B41*, 1651.

(8) (a) Halvorson, K. E. M.S. Thesis, Washington State University, 1989. (b) Willett, R. D. Unpublished results.

(9) Harris, G. S.; Inglis, F.; McKechinie, J.; Cheung, K. K. *J. Chem. Soc., Chem. Commun.* **1967**, 442.

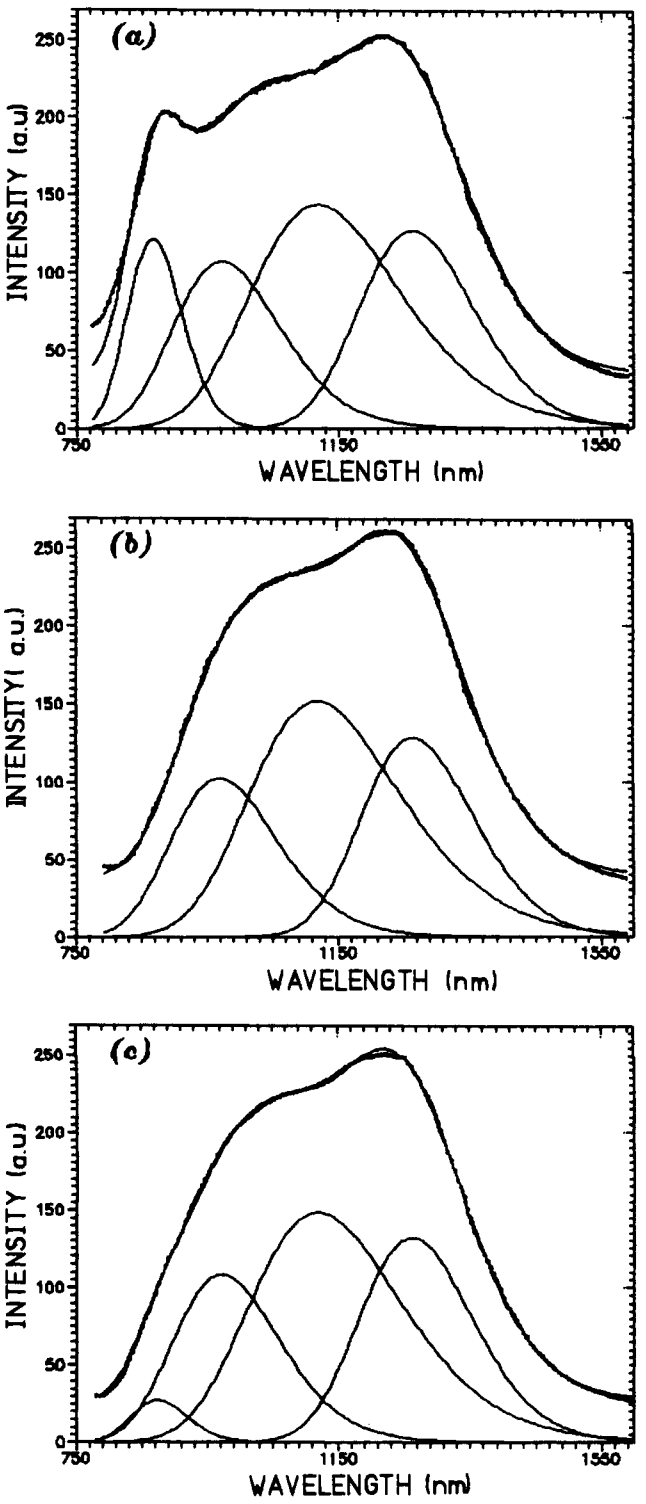

Figure 5. Calculated electronic spectra using a Gaussian line shape showing the components of each d–d transition for the purple crystal sample: (a) $\vec{E}$ parallel to $\vec{b}$; (b) $\vec{E}$ perpendicular to $\vec{b}$; (c) unpolarized spectrum.

region 300–800 nm at 650, 570, 450 (shoulder), and 385 nm (15 400, 17 540, 22 220, and 25 970 cm^{-1}); an additional band appeared at 277 nm (36 000 cm^{-1}). These bands, according to the literature,[10] are associated with ligand-to-metal charge-transfer transitions, since the d–d transitions are expected in the near-infrared region in the case of the $[CuBr_4]^{2-}$ chromophore.

(10) (a) Braterman, P. S. *Inorg. Chem.* **1963**, *2*, 448–452. (b) Marcotrigiano, G.; Menabue, L.; Pellacani, G. C.; Saladini, M., *Inorg. Chim. Acta* **1979**, *34*, 43. (c) Hathaway, B. J.; Billing, D. E. *Coord. Chem. Rev.* **1970**, *5*, 143.

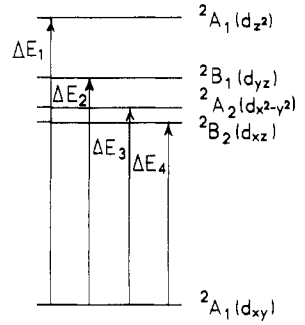

Figure 6. Schematic energy level diagram for the d states. (The Cu d-orbital parentage of the half-occupied levels is given in parentheses.)

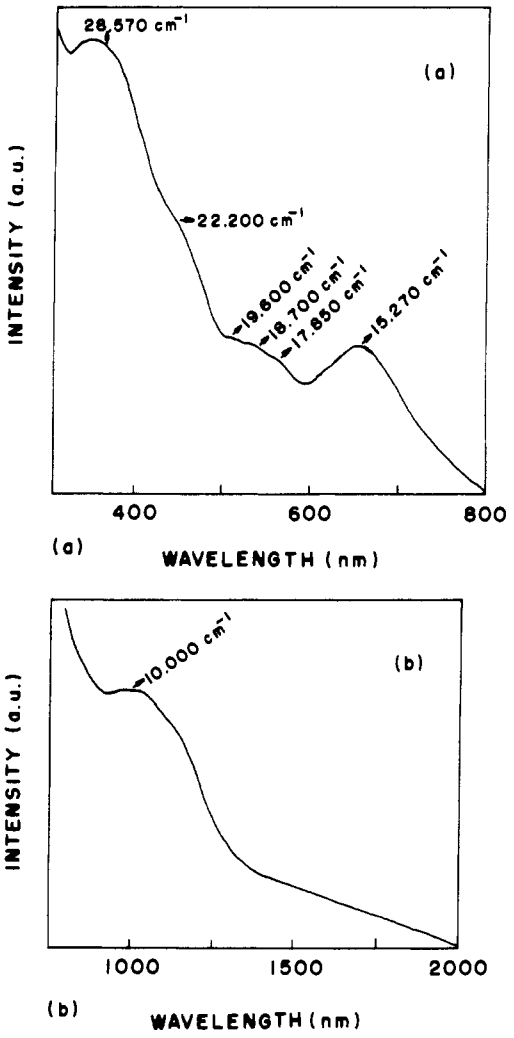

Figure 7. Electronic spectra of the olive green compound: (a) in the 300–800-nm region; (b) in the 750–2000-nm region (fluorolube mull).

Single-crystal polarized spectra in the near-IR region (750–1600 nm) are shown in Figure 4. The spectra were recorded with the electric field vector, $\vec{E}$, of the incident beam parallel and perpendicular to the monoclinic b axis. For $\vec{E}$ parallel to $\vec{b}$, three band maxima are observed around the wavelengths 890, 1055, and 1220 nm, while for $\vec{E}$ perpendicular to $\vec{b}$, only two maxima are observed (1055 and 1220 nm). These spectra correspond to polarization parallel and perpendicular to the C_2 axis of the $[CuBr_4]^{2-}$ anion, respectively. The latter contains components of both x and y polarization. For the comparison purposes, the unpolarized spectrum is also presented in Figure 4. The observed transition energies are in the range anticipated on the basis of the spectra of the analogous $[CuCl_4]^{2-}$ species with similar average trans angles.[6]

Using a simulation program with Gaussian line shape,[11] it was

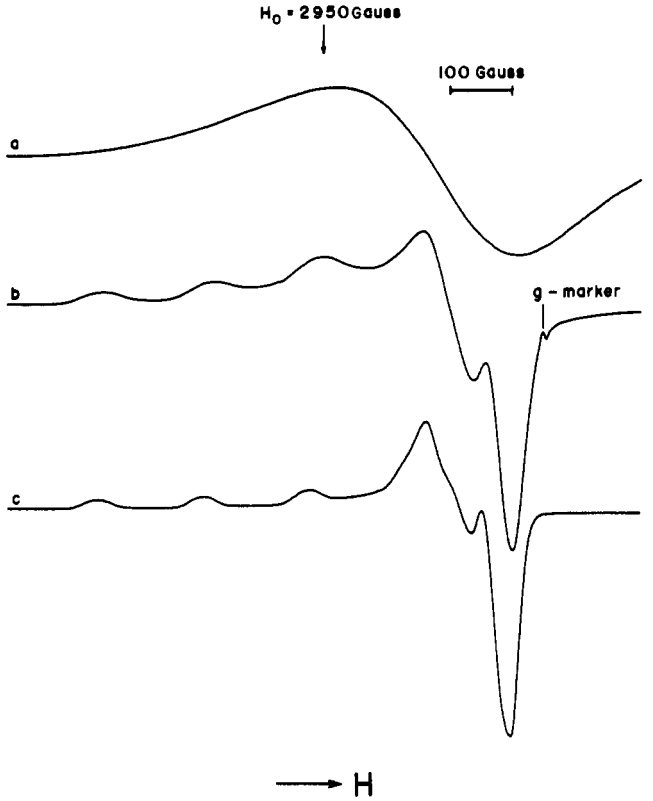

Figure 8. EPR spectra of the powder samples measured at liquid-N_2 temperature: (a) for $(Ph_3AsOH)_2[CuBr_4]$; (b) for $[Cu(Ph_3AsO)_4][CuBr_4]$; (c) for a polycrystalline sample containing only the $[Cu(Ph_3AsO)_4]^{2+}$ cation.[1] The small high-field line is due to a Cr^{3+}:MgO marker (g = 1.9797). The modulation amplitude was 4.0 G peak to peak, and the microwave power was set at 10 mW.

possible to identify all of the d–d transitions of the $[CuBr_4]^{2-}$ anion (see Figure 5a–c). For $\vec{E}$ parallel to $\vec{b}$, four transitions were identified, corresponding to the expected splitting of the ^2E level in D_{2d} symmetry into nondegenerate $^2B_1$ and $^2B_2$ levels in C_{2v} symmetry, due to the orthorhombic distortion. The high-energy, strongly polarized transition observed at 11 490 cm^{-1} (870 nm) is assigned to the $^2A_1 \rightarrow {}^2A'_1$ transition (Figure 6). The other three bands are also observed in the $\vec{E}$ perpendicular to $\vec{b}$ polarization. The ordering of the three intermediate energy levels cannot be unambiguously assigned from the observed spectra, since vibronic coupling obscures the simple dipole selection rules. However, on the basis of the structural characteristics, it is expected that the splitting of the $^2B_1$ and $^2B_2$ levels may be quite large. The ordering indicated in Figure 6 is based on the analysis of the EPR g values (vide infra).

The electronic spectra of the olive green powder compound are shown in Figure 7a,b. In the visible–UV region of 300–800 nm, bands at 655 nm (15 270 cm^{-1}), shoulders at 17 850, 18 700, 19 600, and 22 200 cm^{-1} and another band at 350 nm (28 570 cm^{-1}) are observed (Figure 7b). The bands in the near-IR region around 10 000 cm^{-1} are identified with the d–d transitions of the $[CuBr_4]^{2-}$ anion on the basis of the comparison with the spectrum of the purple complex. The bands at 15 270, 17 850, and 18 700 cm^{-1} arise from an overlap of the d–d transitions of the cation, as seen by comparison with the spectra obtained for previously reported complexes containing the $[Cu(Ph_3AsO)_4]^{2+}$ cation,[1] and the low-lying charge-transfer bands of the $[CuBr_4]^{2-}$ anion. The bands above 19 600 cm^{-1} are a superposition of ligand-to-metal charge-transfer bands characteristic of the anion and the cation.

EPR Spectra. The EPR powder spectra of these two complexes are presented in Figure 8a,b. The spectrum of the purple complex presents a broad line shape with an approximately axial symmetry, and the olive green sample shows a superposition of two kinds of paramagnetic species. In Figure 7c, the powder spectrum of the $[Cu(Ph_3AsO)_4]^{2+}$ cation (from ref 1) is shown for comparison purposes. From the similarity of the g values and hyperfine splitting exhibited by the two spectra in Figure 8a,b, it is reasonable to assume that the olive green sample also contains this cation. This fact reinforces the interpretation of the electronic spectral data of the olive green compound in terms of the $[Cu(Ph_3AsO)_4]^{2+}$ and $[CuBr_4]^{2-}$ chromophores.

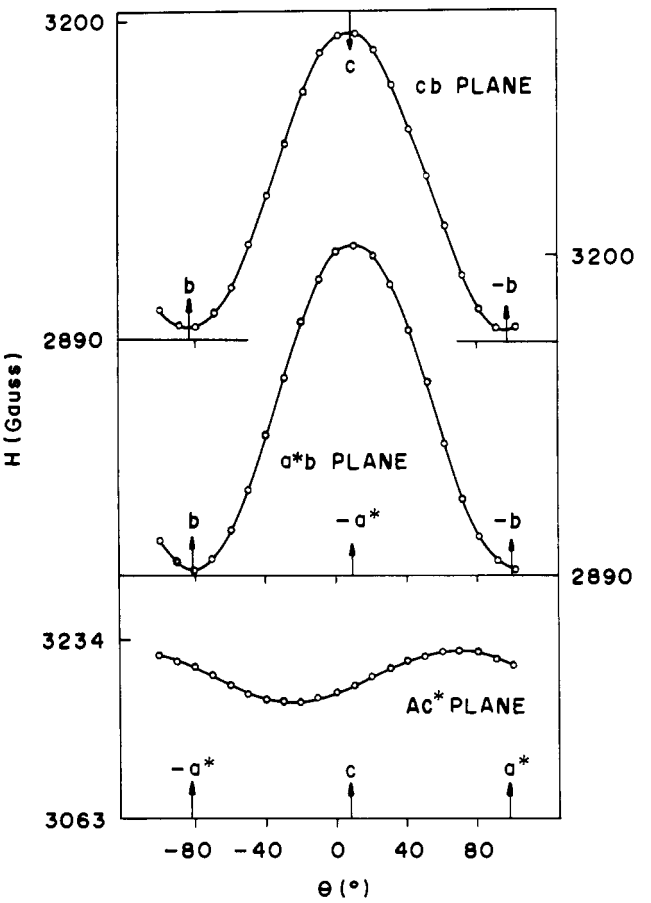

Figure 9. Angular variation of the EPR spectra of the $(Ph_3AsOH)_2[CuBr_4]$ complex using the same single crystal utilized to record the polarized electronic spectra. The continuous lines are the resonance fields calculated by employing the best least-squares g values in Table IV.

Table IV. Electronic d–d Transition Assignments and EPR Parameters for the $[CuBr_4]^{2-}$ Anion in $(Ph_3AsOH)_2[CuBr_4]$

transition	energy, 10^3 cm^{-1}	g values	reduction factors
$d_{z^2} \rightarrow d_{xy}$	11.49 (4)	g_x = 2.0788 (3)	r_x = 0.367
$d_{yz} \rightarrow d_{xy}$	10.30 (2)	g_y = 2.0446 (3)	r_y = 0.270
$d_{x^2-y^2} \rightarrow d_{xy}$	8.94 (2)	g_z = 2.2749 (3)	r_z = 0.360
$d_{xz} \rightarrow d_{xy}$	7.94 (4)		

The EPR spectra for a single crystal of the purple compound was measured in three orthogonal planes, and the angular variation of the resonance fields is presented in Figure 9. The spectra display only a single broad line with anisotropic line width variations between 170 and 300 G. The g tensor was obtained and diagonalized. The b monoclinic axis is coincident with the z principal axis of the g tensor. The g-value variation in the a^*c plane, though small, is consistent with the distortion of the $[CuBr_4]^{2-}$ anion from D_{2d} symmetry. Although the directions associated with g_x and g_y are not precisely coincident with the molecular x and y directions defined above, they are close enough to validate the assumption that the electronic structure characteristics are closely associated with the molecular geometry. The EPR parameters are summarized in Table IV.

Surprisingly, very few detailed studies on undiluted $[CuX_4]^{2-}$ systems have been carried out. For the $[CuBr_4]^{2-}$ anion, a previous study on $(piperidinium)_2[CuBr_4]$ yielded principal g-tensor components of g_x = 2.045, g_y = 2.063, and g_z = 2.290 for an average

(11) Melo, L. B. M.; Tabak, M.; Nascimento, O. R. *Quim. Nova*, in press.

trans angle of 130.9°. This is in reasonable agreement with the result found here.

The molecular EPR g values can be related to the d electron energy levels through the simple relationships[10]

$$g_z = g_0 - r_z[8\lambda/\Delta E_2] \qquad \Delta E_2 = {}^2A_2 - {}^2A_1$$

$$g_y = g_0 - r_y[2\lambda/\Delta E_3] \qquad \Delta E_3 = {}^2B_1 - {}^2A_1$$

$$g_x = g_0 - r_z[2\lambda/\Delta E_4] \qquad \Delta E_4 = {}^2B_2 - {}^2A_1$$

where λ is the spin-orbit coupling parameter for the Cu(II) ion and the r_i values are so-called reduction factors. They represent the effect of delocalization of the d electrons into the ligand orbitals. The energy level assignments were made so as to give as uniform values as possible for the reduction factors. This leads to the energy level scheme illustrated in Figure 6.

A summary of the spectral and the EPR data is presented in Table IV. The difference between g_x and g_y confirms the presence of a rhombic distortion as expected from the crystallographic data. This is the consequence of the substantial splitting (2360 cm^{-1}) between the $^2B_1$ and $^2B_2$ levels. This is not surprising in light of the nearly 0.1-Å difference between the Cu-Br(1) and Cu-Br(2) bond lengths, as well as the 17° difference in the respective *trans*-Br-Cu-Br angles. The supposition that the $^2B_1$ level (unpaired electron in a d_{yz}-type orbital) lies higher in energy than the $^2B_2$ level (a d_{xz}-type orbital) is based upon the fact that the Cu-Br(2) distance is shorter than the Cu-Br(1) distance.

The g values are substantially smaller than those observed for $[CuCl_4]^{2-}$ anions with similar trans angles (cf. Gaura et al.[12]). The reduction factors are also smaller than those normally observed for copper(II) chloride complexes. These small values for the reduction factor are related to the large ligand spin-orbit coupling constants for the Br atoms and to the presence of low-lying ligand → metal charge-transfer levels. Both lead to a reduction of the deviations of g values from the free electron value.[13] The lack of resolvable hyperfine structure even in the single-crystal EPR spectra of $(Ph_3AsOH)_2[CuBr_4]$ indicates the presence of the significant dipolar interaction between $[CuBr_4]^{2-}$ anions.

Acknowledgment. This research work was supported by NSF Grant DMR-8803382 and the Brazilian Financial Agencies FINEP and CNPq. Acknowledgment is made to The Boeing Co. and to the NSF, through the Grant CHE-8408407, for the establishment of the X-ray diffraction facility.

Registry No. $(Ph_3AsOH)_2[CuBr_4]$, 139312-27-9; $[Cu(Ph_3AsO)_4][CuBr_4]$, 139312-26-8.

Supplementary Material Available: Tables of data collection and refinement parameters, hydrogen atom positions, and anisotropic thermal parameters and a packing diagram (4 pages); a table of observed and calculated structure factors (14 pages). Ordering information is given on any current masthead page.

(12) Gaura, R. M.; Stein, P.; Willett, R. D.; West, D. X. *Inorg. Chim. Acta* **1982**, *60*, 213.
(13) Wong, R. J.; Willett, R. D. *J. Magn. Reson.* **1981**, *42*, 446.

Contribution from the Department of Chemistry, University of Oregon, Eugene, Oregon 97403, and Du Pont, Central Research and Development, Experimental Station, Wilmington, Delaware 19880-0356

Two New Barium-Copper-Ethylene Glycol Complexes: Synthesis and Structure of $BaCu(C_2H_6O_2)_n(C_2H_4O_2)_2$ (n = 3, 6)

Craig P. Love,[1a] Charlie C. Torardi,[1b] and Catherine J. Page*,[1a]

Received October 7, 1991

Two crystalline barium-copper-ethylene glycol complexes have been isolated and structurally characterized by single-crystal X-ray diffraction. The solution-phase complex has also been investigated as a molecular precursor for use in sol-gel synthesis of high-temperature superconductors. The first crystalline form has the formula $BaCu(C_2H_6O_2)_6(C_2H_4O_2)_2$ (**1**) and has been isolated directly from ethylene glycol solutions of the barium-copper salt. Crystallographic data for **1** are as follows: monoclinic space group *Cc* (No. 9), a = 12.103 (6) Å, b = 13.527 (3) Å, c = 17.091 (8) Å, β = 93.17 (2)°, V = 2793.8 Å^3, Z = 4, R = 0.030. In this molecule, copper is coordinated to the four oxygens of two ethylene glycolate ligands in a nearly square planar geometry. Barium is coordinated by three bidentate ethylene glycol molecules and three monodentate ethylene glycol molecules; the 9-fold coordination resembles a trigonal prism with each rectangular face capped. Copper and barium moieties do not share any ethylene glycol or glycolate oxygens; they are bound by hydrogen bonding to form linear chains. The second crystal type has formula $BaCu(C_2H_6O_2)_3(C_2H_4O_2)_2$ (**2**). It was prepared via crystallization of the mixed-metal alkoxide from an ethylene glycol/methyl ethyl ketone solution. Crystallographic data for **2** are as follows: monoclinic space group $P2_1/n$ (No. 14), a = 12.127 (4) Å, b = 11.913 (1) Å, c = 12.540 (4) Å, β = 102.47 (1)°, V = 1768.9 Å^3, Z = 4, R = 0.025. As for **1**, the copper is coordinated to four oxygen atoms of two ethylene glycolate ligands in a nearly square planar arrangement. Barium is 8-coordinate in a distorted cubic geometry. It is coordinated to three bidentate ethylene glycol molecules and shares two of the oxygen atoms bound to the copper (one from each coordinated ethylene glycol) to form a discrete molecular barium-copper complex.

Introduction

Alkoxides of yttrium, barium, and copper have recently attracted interest as molecular precursors for the sol-gel synthesis of new high-temperature superconductors, such as $YBa_2Cu_3O_{7-\delta}$.[2-8] Sol-gel synthetic routes to high-temperature superconductors offer many potential advantages over conventional solid-state reactions, including lower processing temperatures, high homogeneity and purity, and the ability to fabricate the intermediate viscous sol into a variety of forms, including thin films or fibers.

The alkoxide sol-gel synthetic route is a multistep process which begins with a solution-phase mixture of metal alkoxides in a nonaqueous solvent. The metal alkoxide solution is hydrolyzed to form a colloidal sol or an oxide gel (depending on the conditions of hydrolysis) which can subsequently be dried and fired at relatively low temperatures to form crystalline oxides. The first step

(1) (a) University of Oregon. (b) Du Pont.
(2) Kordas, G. *J. Non-Cryst. Solids* **1990**, *21*, 436.
(3) Catania, P.; Hovnanian, N.; Cot, L.; Pham Thi, M.; Kormann, R.; Ganne, J. P. *Mater. Res. Bull.* **1990**, *25*, 631.
(4) Hayri, E. A.; Greenblatt, M.; Ramanujachary, K. V.; Nagano, M.; Oliver, J.; Miceli, M. J.; Gerhart, R. *J. Mater. Res.* **1989**, *4*, 1099.
(5) Horowitz, H. S.; McLain, S. J.; Sleight, A. W.; Druliner, J. D.; Gai, P. L.; VanKavelaar, M. J.; Wagner, J. L.; Biggs, B. D.; Poon, S. J. *Science* **1989**, *243*, 66.
(6) Hirano, S.; Hayashi, T.; Miura, M.; Tomonaga, H. *Bull. Chem. Soc. Jpn.* **1989**, *62*, 888.
(7) Zheng, H.; Mackenzie, J. D. *Mater. Lett.* **1988**, *7*, 182.
(8) Shibata, S.; Kitagawa, T.; Okazake, H.; Kimura, T. *Jpn. J. Appl. Phys.* **1988**, *27*, L646.

0020-1669/92/1331-1784$03.00/0